

Title

***Sleeping Beauty* insertional mutagenesis screen identifies the pro-metastatic roles of *CNPY2* and *ACTN2* in hepatocellular carcinoma tumor progression**

Authors

Lilian H. Lo^{1,2}, Coco Y. Lam^{1,2}, Jeffrey C. To^{1,2}, Cynthia H. Chiu^{1,2} & Vincent W. Keng^{1,2,3*}

Affiliations

¹State Key Laboratory of Chinese Medicine and Molecular Pharmacology (Incubation), Shenzhen 518057, China. ²Department of Applied Biology and Chemical Technology, The Hong Kong Polytechnic University, Hung Hom, Kowloon, Hong Kong SAR. ³State Key Laboratory of Chemical Biology and Drug Discovery, The Hong Kong Polytechnic University, Hung Hom, Kowloon, Hong Kong SAR.

Corresponding author

*Correspondence should be addressed to V.W.K.

Vincent W. Keng

Department of Applied Biology and Chemical Technology, State Key Laboratory of Chemical Biology and Drug Discovery, The Hong Kong Polytechnic University, Hung Hom, Kowloon, Hong Kong SAR.

Tel: +852-3400-8728

Fax: +852-2364-9932

Email: vincent.keng@polyu.edu.hk

Keywords

Hepatocellular carcinoma; Sleeping Beauty; forward genetic screen; CNPY2; ACTN2; metastasis

Abstract

A forward genetic Sleeping Beauty (*SB*) insertional mutagenesis screen, followed by high-throughput transcriptome sequencing, was used to identify driver genes responsible for hepatocellular carcinoma (HCC)-associated metastasis. Using RNA-sequencing (RNA-seq) to identify transposon-endogenous transcriptome fusion genes, the phylogenetic lineage between the parental liver tumor and secondary metastasis can be determined to provide mechanistic insight to genetic changes involved in the metastatic evolution process. In the current study, two novel candidate genes were identified to be potentially involved in HCC-associated metastatic progression, canopy FGF signaling regulator 2 (*Cnpy2*) and actinin alpha 2 (*Actn2*). Transposon-*Cnpy2* fusion transcripts were identified in both primary liver tumors and lung metastases. Its significant association with clinicopathological characteristics and correlated gene enrichment in metastasis-related mechanisms suggest its potential role in modulating local invasion and angiogenesis. Other known driver genes for human HCC that can also promote metastatic progression include epidermal growth factor receptor (*Egfr*) and RNA imprinted and accumulated in nucleus (*Rian*). Metabolic pathway related gene carbamoyl phosphate synthetase (*Cps1*) was identified to play an important role in early HCC development, while cell junction-related pathway gene Rac family small GTPase 1 (*Rac1*) was identified to play an important role in both HCC and pro-metastatic progression. Importantly, actinin alpha 2 (*Actn2*) was identified exclusively in the secondary metastasis site and its role in HCC-related metastatic process was elucidated using *in vitro* approaches. *ACTN2*-overexpression in human liver cancer cells displayed enhanced cellular motility and invasion abilities, indicating its possible function in later stage of metastasis, such as extravasation and lung colonization.

Introduction

A *SB* insertional mutagenesis forward genetic screen was performed in order to identify novel genes responsible for the metastatic process in HCC and further understand their underlying molecular mechanism(s). This screen successfully induced HCC formation and generated secondary lung metastases, recapitulating the human disease. RNA-seq was employed to identify transposon-endogenous transcriptome fusion genes and determine the phylogenetic lineage between parental liver tumor and secondary metastasis. A total of 298 transposon-endogenous gene fusion transcripts were identified in liver tumors and lung metastases obtained from the same animal. After further informatic analyses using Ingenuity Pathway Analysis (IPA) and Database for Annotation, Visualization and Integrated Discovery (DAVID), many pathways associated with tumorigenesis and metastasis in human HCC were identified. Overlapping transposon-endogenous gene fusion transcripts in both primary liver tumors and secondary lung metastases include known driver genes for human HCC development and tumor growth such as *EGFR* [1], and maternally expressed 8, small nucleolar RNA host gene (*MEG8*, also known as *Rian* in rodents) [2]. Metabolic pathways such as alanine metabolism and urea cycle have been suggested to play an important role in early HCC development. Notably, *Cnpy2* and *Actn2* were identified as novel metastasis-associated candidate genes responsible for different stages of tumor spread. The association between *CNPY2* overexpression with aggressive outcome in HCC, together with the predicted metastatic pathways by DAVID, suggest the potential pro-metastatic role of *CNPY2*. Transposon fusion with *Actn2* transcripts were found exclusively in lung metastases. Upon further validation using *in vitro* methods, the novel role of *ACTN2* was confirmed for its pro-metastatic role in HCC tumorigenesis.

Materials and methods

SB insertional mutagenesis forward genetic screen

The transgenic mice used for this screen have been previously described [3,4]. Experimental male mice have an active *SB* insertional mutagenesis system, while male mice without a functional *SB* insertional mutagenesis system were used as controls. All animals received human care and the study protocols have been approved by the Animal Subjects Ethic Subcommittee of The Hong Kong Polytechnic University.

Liver tumor analyses

The entire mouse liver was harvested, weighed and rinsed with cold phosphate buffered saline (PBS). Tumor nodules were counted, isolated and divided for RNA and histological analyses. RNA isolation was done using Trizol reagent (Life Technologies) according to the manufacturer's protocol. Formalin fixed-paraffin embedded sections from various tissues were sectioned at 5 microns using a standard microtome (Leica), mounted and heat-fixed onto glass slides for hematoxylin-eosin (HE) and/or immunohistochemical (IHC) analyses.

IHC analyses

Tissue section slides were dewaxed by xylene (Leica) and rehydrated through a gradual decrease in ethanol concentration. Antigen epitope retrieval with unmasking solution (Vector Laboratories), removal of endogenous peroxidases with 3% hydrogen peroxide and blocking using M.O.M. mouse immunoglobulin-blocking reagent (Vector Laboratories) for 1 hour were performed on the tissue sections, followed by overnight incubation of primary antibody at 4°C in a humidified chamber. The sections were washed with PBS before incubation with horseradish peroxidase-secondary antibody for one hour. After PBS washing, the sections were treated with freshly prepared DAB substrate (Vector Laboratories) and allowed for

adequate signal development before terminating the reaction with water. Antibodies in various concentrations as listed: SB transposase (R&D Systems) (1:100); FAH (Abcam) (1:100).

RNA-seq

RNA-seq and bioinformatic analyses were outsourced to Beijing Genomics Institute (BGI).

RT-PCR

First strand cDNA synthesis was performed using the PrimeScript RT Master Mix (Takara) as described by the manufacturer using 1 µg total RNA as template. Both reactions with (RT+) and without (RT-) the reverse transcriptase were performed for all the samples. Subsequent PCR was performed using 1 µl of the cDNA as template with various primer pairs. Primer sequences and amplicon sizes for Sleeping Beauty transposase (*SB11*), albumin (*Alb*), fumarylacetoacetate hydrolase (*Fah*) and actin beta (*Actb*) have been previously described [3,4]. Primer sequences for transposon-endogenous gene fusion transcript genotyping include SV40-polyA-Reverse 5'-TGCTTTATTTGTGAAATTTGTGATGCTATTG-3'; MSCV SD 5'-CTACTAGCACCAGAACGCCC-3'; *Egfr* Ex23 Forward 5'-GTGTCACTGTGTGGGAAGTATGACCT-3'; *Egfr* Ex24 Reverse 5'-CTGGATAACAAGGTAGCGCTGTGGGTC-3'; *Egfr* Ex26 Forward 5'-AGTGCAACTAGCAACAATTC-3'; *Egfr* Ex27 Reverse 5'-AGGTACAGGGAGGAATGCGT-3'; *Actn2* Ex13 Forward 5'-CACGATGCTGTGAACGTCAA-3'; *Actn2* Ex15 Reverse 5'-TGGCCTTGAAGTCTCATGT-3'; *Actn2* Ex16 Forward 5'-TGCTAATGAGCGTCTGCGG-3'; *Actn2* Ex17 Reverse 5'-TCGTGTGCTTGTGTCGAAG-3'. PCR conditions were 25 to 30 cycles to avoid amplicon saturation.

Cell culture and transfection conditions

The human HCC cell line MHCC97L (kind gift from Dr Terence K. Lee, The Hong Kong Polytechnic University) was cultured in Dulbecco's modified Eagle's Medium, supplemented with 10% fetal bovine serum and 1% antibiotic-antimycotic, in a humidified 5% CO₂ incubated at 37 °C. All cell culture media and reagents were purchased from Life Technologies.

The piggyBac (*PB*) transposon system was used to stably integrate and overexpress the truncated *ACTN2* (TAC), full-length *ACTN2* (AC) or control orange fluorescent protein (*OFP*) cDNAs in MHCC97L cells. Briefly, *ACTN2* cDNA (OriGene Technologies, RC208531, NM_001103) was used as template for high fidelity PCR using primer pairs *KpnI*-Kozak-Flag-*ACTN2* forward 5'-CAGGGTACCGCCACCATGGACTACAAAGACGATGACGACAAGCTTGCGGCCAAC CAGATAGAGCCCGGCGT-3' and *EcoRV*-*ACTN2* reverse 5'-CAGTCGATATCTCACAGATCGCTCTCCCCGT-3', and cloned into the *PB* transposon expression vector to generate pPB/SB-AC-GFP-Puro using the Gateway cloning system (Thermo Fisher). *ACTN2* cDNA (OriGene Technologies) was also used as template for high fidelity PCR using primer pairs *KpnI*-Kozak-FLAG-Truncated *ACTN2* forward 5'-GGTACCGCCACCATGGACTACAAAGACGATGACGACAAGCTTGCGGCCATGAGT CTGATCACTGCGCA-3' and *EcoRV*-Truncated *ACTN2* reverse 5'-GATATCTCACAGATCGCTCTCCCCGT-3', and cloned into *PB* transposon expression vector using the similar method to generate pPB/SB-TAC-GFP-Puro. A control expression vector containing *OFP* was generated using the similar method to yield pPB/SB-OFP-Puro. pPB/SB-AC-GFP-Puro, pPB/SB-TAC-GFP-Puro or pPB/SB-OFP-Puro was then co-transfected with *PB* transposase vector into MHCC97L cells using ViaFect transfection reagent

(Promega) according to the manufacturer's instruction. Post-transfection selection using puromycin (Thermo Fisher) was performed to enrich for stably transfected cells.

Transwell migration and matrigel invasion chamber assays

Transwell migration inserts were purchased from Millicell and matrigel invasion chambers were from Corning. Human liver cancer cell line in serum-free medium (5×10^4 cells) were placed in upper chamber and serum-containing medium was added to the lower chamber according to the manufacturer's instructions. After 48 hours incubation, cells that have either migrated or invaded into the lower chamber were fixed with 4% paraformaldehyde in PBS and stained lightly with haematoxylin. Migrated cells were imaged at 100X magnification and counted using ImageJ 1.40J software (NIH, Maryland, USA).

Result

SB insertional mutagenesis system induced HCC development and metastasis

A forward genetic *SB* insertional mutagenesis screen was performed to discover novel genes involved in HCC development and metastasis (**Fig. 1A**). Experimental mice displayed early liver tumor formation at 150- to 203-days with preneoplastic nodules, with increased tumor burden upon further aging to 305- to 316-days (**Fig. 1B**). In contrast, no observable liver nodules were observed at both timepoints in control cohorts. Importantly, approximately 14% of experimental mice ($n = 5$) displayed lung metastases (**Fig. 1C**). Active *SB* mutagenesis system and expression of liver-specific fumarylacetoacetate hydrolase (*Fah*) were confirmed in tumors at both the mRNA and protein levels (**Fig. 2A** and **2B**, respectively).

Transposon-fusion transcript enriched pathways from liver tumors recapitulate human HCC

A subset of primary liver tumors ($n = 5$) and lung metastases ($n = 4$) taken from the same experimental animal were analyzed by RNA-seq to identify the transposon-endogenous gene fusion transcripts. There were 167 (primary tumors) and 140 (secondary lung metastases) fusion transcripts detected, where 9 overlapping fusion transcripts were observed (**Supplementary Fig. 1A**, **Supplementary Table 1** and **Supplementary Table 2**).

DAVID and IPA were used to determine mechanistic pathways enriched by transposon fusion transcripts in liver tumors and lung metastases separately. Using DAVID, enriched pathways associated with primary tumor were arginine biosynthesis and protein processing in endoplasmic reticulum (**Supplementary Table 3**). Pathways suggested by IPA were mainly metabolic related signaling, such as alanine metabolism, urea cycle and nicotinamide adenine dinucleotide (NAD) metabolism (**Supplementary Table 4**). Arginine biosynthesis and urea cycle both share the same pathway with the same set of liver-specific transposon-fusion transcripts, namely *Cps1* and arginase 1 (*Arg1*). *CPS1* genetic alterations have been reported

in 9% of human HCC patients (TCGA, $n = 360$), in which 29% of these patients ($n = 10$) harbor gene mutations such as missense and truncating mutation (**Supplementary Fig. 1B**). Importantly, downregulated *CPS1* expression in HCC patients greatly reduced the overall (**Supplementary Fig. 1C**) and disease-free (**Supplementary Fig. 1D**) survival rates using GEPIA.

Common transposon-Egfr fusion transcripts in primary liver tumors and secondary lung metastases

The top overlapping transposon-endogenous gene fusion transcripts in both primary liver tumors and secondary lung metastases are known driver genes for human HCC development and tumor growth: *EGFR*, *CNPY2* and *MEG8* (known as *Rian* in rodents) (**Supplementary Table 1**). *Egfr*-transposon fusion transcripts were most frequently reported in the RNA-seq data, where *Egfr* exon 24 spliced with the mutagenic transposon splice acceptor/polyadenylation tail (SA/pA), resulting in a premature truncation lacking the carboxy terminus (**Fig. 3A** and **3B**). RT-PCR genotyping on remaining non-sequenced liver and metastatic tumors also confirmed the common *Egfr*-transposon fusion truncation (**Fig. 3E**). The endogenous expression of *Egfr* after the fusion site was notably reduced compared with expression levels before the transposon-*Egfr* exon 24 fusion site (**Fig. 3E**).

CNPY2 as a novel metastatic candidate gene

Genetic alterations in *CNPY2* have been reported in 10% of human HCC patients (TCGA), in which 40% of these patients ($n = 14$) displayed either macro- or micro-vascular invasion (**Supplementary Fig. 2A**). *CNPY2* overexpression in HCC is significantly associated with poorer overall and disease-free survival (**Supplementary Fig. 2B**). Using UALCAN, *CNPY2* expression is significantly higher in primary tumors compared with normal liver, and its

expression is significantly associated with tumor grade and stage (**Supplementary Fig. 2C**). Using Gene Expression Omnibus (GEO) database, *CNPY2* overexpression was significantly detected in metastatic HCCs and lung metastases, compared with early stage HCC (GSE40367) (**Supplementary Fig. 2D**) [5]. DAVID analyses on *CNPY2*-positively correlated genes predicted its involvement in DNA replication, ribosome, spliceosome and proteasome, confirming the enhanced cell proliferation seen in *CNPY2*-altered cancers (**Supplementary Table 7**). Focal adhesion, regulation of actin cytoskeleton, RAP1 signaling pathway, HIF1 signaling and VEGF pathways were enriched by *CNPY2*-negatively correlated genes, suggesting its potential role in regulating the cell adhesion, invasion and angiogenesis (**Supplementary Table 8**). These data suggest that *CNPY2* accumulation is potentially responsible for the acquisition and progression of metastasis in HCC tumorigenesis.

Transposon-fusion transcript enriched pathways from lung metastases

Using DAVID, enriched pathways associated with secondary lung metastases were FoxO signaling pathway, adherens junction and PI3K-AKT signaling pathway (**Supplementary Table 3**). Pathways suggested by IPA were ILK signaling, glucocorticoid receptor signaling and epithelial adherens junction signaling (**Supplementary Table 4**). Both pathway analysis tools suggested adherens junction signaling in secondary lung metastases, responsible for cell-cell adhesion via actin filaments during metastasis. Using UALCAN, increased *RAC1* expression was significantly associated with more advanced HCC stage (**Supplementary Fig. 3A**) and tumor grade (**Supplementary Fig. 3B**). Increased *RAC1* expression reduces both overall (**Supplementary Fig. 3C**) and disease-free (**Supplementary Fig. 3D**) survival rates in GEPIA. Its genetic alteration has been reported in 12% of HCC patients (TCGA), in which 30% of these patients ($n = 13$) displayed either macro- or micro-vascular invasion

(**Supplementary Fig. 3E**). Moreover, one case was reported as M1 using the AJCC staging system (**Supplementary Fig. 3F**).

ACTN2 as a novel metastatic candidate gene

From the RNA-seq lung metastases exclusive transposon-endogenous fusion transcripts, *Actn2* had the second highest total reads supporting the fusion event exclusively in lung metastases and was further validated (**Supplementary Table 2**). Interestingly, transposon insertion occurred in *Actn2* intron 14 and the fusion transcript resulted between the transposon splice donor (SD) and *Actn2* exon 15, resulted in a gain-of-function truncated transcriptional activation by the murine stem cell virus 5' long terminal repeat (MSCV 5' LTR) in the oncogenic transposon (**Fig. 3C and 3D**). RT-PCR genotyping confirmed the transposon-*Actn2* fusion and transcriptional activation in 94% of RNA-seq and non-sequenced lung metastases ($n = 31$) (**Fig. 3E**). Notably, *Actn2* was identified by both DAVID and IPA as one of the components involved with adherent junctions and responsible in actin cytoskeleton regulation during metastasis (**Supplementary Table 5 and Supplementary Table 6**).

In HCC patients (TCGA), 24% of cases ($n = 87$) harbor *ACTN2* genetic alterations involving mainly mRNA overexpression and gene amplification (**Supplementary Fig. 4A**). In TCGA, >50% of HCC tumor >T1 stage (**Supplementary Fig. 4A**) and 34% of invasive cases (**Supplementary Fig. 4B**) were detected with *ACTN2* genetic alterations. Importantly, 3 M1 stage HCCs displayed *ACTN2* dysregulation (**Supplementary Fig. 4C**). UALCAN recorded an increased *ACTN2* expression in higher HCC cancer stage (**Supplementary Fig. 4D**). Using GEO database, significantly increased *ACTN2* mRNA expression was detected in liver tumors compared to their adjacent normal tissue (GSE54236) (**Supplementary Fig. 4E**) [6-8]. Significantly increased *ACTN2* mRNA expression was also detected in lung metastases compared with early HCC (GSE40367) (**Supplementary Fig. 4F**).

Effect of ACTN2-overexpressing variants on cellular invasion and migration

In order to elucidate the functional roles and differences in metastatic abilities between truncated *ACTN2* (TAC) and full-length *ACTN2* (AC), the *PB* transposon system was used as a gene delivery tool to stably overexpress these *ACTN2* variants in MHCC97L cells (**Fig. 4A**). Increased cellular invasion was observed by both variants, represented by increased number of invaded cells (**Fig. 4B**). Interestingly, TAC variant displayed significantly more migrated cells compared with both AC variant and control, while the AC variant showed no significant difference with control (**Fig. 4B**).

Discussion

In this study, conditional activation of *SB* insertional mutagenesis in mouse hepatocytes allowed for the identification of functionally relevant driver genes involved with HCC tumorigenesis, including its associated metastatic process. Using this screening system, HCC-induced metastasis was recapitulated in mice and a total of 298 transposon-endogenous gene fusion transcripts were identified in primary liver tumors and secondary lung metastases.

Findings from genomic to metabolomic approaches demonstrate *CPS1* plays an important role in early HCC development and is a potential HCC biomarker [9-11]. Disruption of intercellular junction dynamics have been reported frequently in tumor metastasis that affect cell adhesion, migration and invasion during epithelial-mesenchymal transition [12-15]. *Rac1* is one of the common components in cell junction-related pathways from both pathway analyses and is frequently reported in liver cancer metastasis [16-18]. *RAC1* controls the endocytosis of E-cadherin (a component in adherens junction) to modulate the cell-cell adhesion and cell motility.

Altered *CNPY2* expression has been frequently reported in many cancer types by contributing to tumor growth [19-21]. *CNPY2* was found to be highly associated with tumor progression in HCC (**Supplementary Fig. 2C**). Data from DAVID on significantly correlated genes reflects the role of *CNPY2* in regulating tumor growth and dissemination (**Supplementary Table 7** and **Supplementary Table 8**). Enrichment in cytoskeleton remodeling, angiogenic pathways, and detection of transposon-fusion transcripts in both liver tumors and lung metastases suggest the potential involvement of *CNPY2* in early stage of metastasis (local invasion and intravasation) (**Fig. 4C**).

Actn2 was also identified as a candidate gene involved in the metastatic process of HCC, where its fusion with *SB* mutagenic transposon upstream of *Actn2* exon 15 was observed exclusively

in 94% of all harvested lung metastases. Transposon-*Actn2* fusion upstream of exon 15 generated a transcriptional activation of the carboxyl-terminus of the CaM domain. Actinin alpha is a dimeric actin cross-linking protein responsible for modulating cross-linking of actin filaments. It is hypothesized that this truncated version of ACTN2 disrupts its dimerized structure, resulting in the dysregulation of actin cytoskeleton structure and changes in cellular shape. *ACTN2* may be involved in later stages of metastasis, such as extravasation and lung-specific colonization (**Fig. 4C**).

In summary, our current study highlighted the potential roles of *CNPY2* and *ACTN2* in the different stages of cancer spread, while *ACTN2*-overexpression in human liver cancer cells confirmed its pro-metastatic role in HCC disease progression.

Acknowledgements

V.W.K. is supported by Research Impact Fund (R5050-18) from the Research Grant Council, Hong Kong Government; Project 82073134 supported by National Natural Science Foundation of China and NSFC/RGC Joint Research Scheme (N-PolyU 503/16). State Key Laboratory of Chemical Biology and Drug Discovery, and Research Project Grants (G-UA94 and 1-ZVLC) funded by the Department of Applied and Chemical Technology, The Hong Kong Polytechnic University.

References

- [1] V.W. Keng, D. Sia, A.L. Sarver, B.R. Tschida, D.H. Fan, C. Alsinet, M. Sole, W.L. Lee, T.P. Kuka, B.S. Moriarity, A. Villanueva, A.J. Dupuy, J.D. Riordan, J.B. Bell, K.A.T. Silverstein, J.M. Llovet, D.A. Largaespada, Sex bias occurrence of hepatocellular carcinoma in Poly7 molecular subclass is associated with EGFR, *Hepatology* (Baltimore, Md.) 57 (2013) 120-130. 10.1002/hep.26004.
- [2] J. Lou, W. Yan, Q.Y. Li, A.K. Zhu, B.Q. Tan, R. Dong, X.Z. Zou, T. Liu, LncRNA MEG8 plays an oncogenic role in hepatocellular carcinoma progression through miR-367-3p/14-3-3zeta/TGFBetaR1 axis, *Neoplasia* (2020). 10.4149/neo_2020_200730N785.
- [3] V.W. Keng, D. Sia, A.L. Sarver, B.R. Tschida, D. Fan, C. Alsinet, M. Sole, W.L. Lee, T.P. Kuka, B.S. Moriarity, A. Villanueva, A.J. Dupuy, J.D. Riordan, J.B. Bell, K.A. Silverstein, J.M. Llovet, D.A. Largaespada, Sex bias occurrence of hepatocellular carcinoma in Poly7 molecular subclass is associated with EGFR, *Hepatology* 57 (2013) 120-130. 10.1002/hep.26004.
- [4] V.W. Keng, A. Villanueva, D.Y. Chiang, A.J. Dupuy, B.J. Ryan, I. Matise, K.A. Silverstein, A. Sarver, T.K. Starr, K. Akagi, L. Tessarollo, L.S. Collier, S. Powers, S.W. Lowe, N.A. Jenkins, N.G. Copeland, J.M. Llovet, D.A. Largaespada, A conditional transposon-based insertional mutagenesis screen for genes associated with mouse hepatocellular carcinoma, *Nat. Biotechnol.* 27 (2009) 264-274. nbt.1526 [pii] 10.1038/nbt.1526.
- [5] Q.H. Ye, W.W. Zhu, J.B. Zhang, Y. Qin, M. Lu, G.L. Lin, L. Guo, B. Zhang, Z.H. Lin, S. Roessler, M. Forgues, H.L. Jia, L. Lu, X.F. Zhang, B.F. Lian, L. Xie, Q.Z. Dong, Z.Y. Tang, X.W. Wang, L.X. Qin, GOLM1 Modulates EGFR/RTK Cell-Surface Recycling to Drive Hepatocellular Carcinoma Metastasis, *Cancer Cell* 30 (2016) 444-458. 10.1016/j.ccell.2016.07.017.

- [6] F. Dituri, R. Scialpi, T.A. Schmidt, M. Frusciante, S. Mancarella, L.G. Lupo, E. Villa, G. Giannelli, Proteoglycan-4 is correlated with longer survival in HCC patients and enhances sorafenib and regorafenib effectiveness via CD44 in vitro, *Cell Death Dis* 11 (2020) 984. 10.1038/s41419-020-03180-8.
- [7] E. Villa, R. Critelli, B. Lei, G. Marzocchi, C. Camma, G. Giannelli, P. Pontisso, G. Cabibbo, M. Enea, S. Colopi, C. Caporali, T. Pollicino, F. Milosa, A. Karampatou, P. Todesca, E. Bertolini, L. Maccio, M.L. Martinez-Chantar, E. Turola, M. Del Buono, N. De Maria, S. Ballestri, F. Schepis, P. Loria, G. Enrico Gerunda, L. Losi, U. Cillo, Neoangiogenesis-related genes are hallmarks of fast-growing hepatocellular carcinomas and worst survival. Results from a prospective study, *Gut* 65 (2016) 861-869. 10.1136/gutjnl-2014-308483.
- [8] I. Zubiete-Franco, J.L. Garcia-Rodriguez, F. Lopitz-Otsoa, M. Serrano-Macia, J. Simon, P. Fernandez-Tussy, L. Barbier-Torres, D. Fernandez-Ramos, V. Gutierrez-de-Juan, S. Lopez de Davalillo, O. Carlevaris, A. Beguiristain Gomez, E. Villa, D. Calvisi, C. Martin, E. Berra, P. Aspichueta, N. Beraza, M. Varela-Rey, M. Avila, M.S. Rodriguez, J.M. Mato, I. Diaz-Moreno, A. Diaz-Quintana, T.C. Delgado, M.L. Martinez-Chantar, SUMOylation regulates LKB1 localization and its oncogenic activity in liver cancer, *EBioMedicine* 40 (2019) 406-421. 10.1016/j.ebiom.2018.12.031.
- [9] H. Liu, H. Dong, K. Robertson, C. Liu, DNA methylation suppresses expression of the urea cycle enzyme carbamoyl phosphate synthetase 1 (CPS1) in human hepatocellular carcinoma, *Am J Pathol* 178 (2011) 652-661. 10.1016/j.ajpath.2010.10.023.
- [10] T.H. Wang, C.H. Wu, C.T. Yeh, S.C. Su, S.M. Hsia, K.H. Liang, C.C. Chen, C. Hsueh, C.Y. Chen, Melatonin suppresses hepatocellular carcinoma progression via lncRNA-CPS1-IT-mediated HIF-1alpha inactivation, *Oncotarget* 8 (2017) 82280-82293. 10.18632/oncotarget.19316.

- [11] T.H. Wang, C.C. Yu, Y.S. Lin, T.C. Chen, C.T. Yeh, K.H. Liang, T.M. Shieh, C.Y. Chen, C. Hsueh, Long noncoding RNA CPS1-IT1 suppresses the metastasis of hepatocellular carcinoma by regulating HIF-1alpha activity and inhibiting epithelial-mesenchymal transition, *Oncotarget* 7 (2016) 43588-43603. 10.18632/oncotarget.9635.
- [12] G. Giannelli, P. Koudelkova, F. Dituri, W. Mikulits, Role of epithelial to mesenchymal transition in hepatocellular carcinoma, *J Hepatol* 65 (2016) 798-808. 10.1016/j.jhep.2016.05.007.
- [13] A. Kim, E.Y. Kim, E.N. Cho, H.J. Kim, S.K. Kim, J. Chang, C.M. Ahn, Y.S. Chang, Notch1 destabilizes the adherens junction complex through upregulation of the Snail family of E-cadherin repressors in non-small cell lung cancer, *Oncol Rep* 30 (2013) 1423-1429. 10.3892/or.2013.2565.
- [14] J. Lin, W. Lin, Y. Ye, L. Wang, X. Chen, S. Zang, A. Huang, Kindlin-2 promotes hepatocellular carcinoma invasion and metastasis by increasing Wnt/beta-catenin signaling, *J Exp Clin Cancer Res* 36 (2017) 134. 10.1186/s13046-017-0603-4.
- [15] E. Lara-Pezzi, S. Roche, O.M. Andrisani, F. Sanchez-Madrid, M. Lopez-Cabrera, The hepatitis B virus HBx protein induces adherens junction disruption in a src-dependent manner, *Oncogene* 20 (2001) 3323-3331. 10.1038/sj.onc.1204451.
- [16] S. Liu, M. Yu, Y. He, L. Xiao, F. Wang, C. Song, S. Sun, C. Ling, Z. Xu, Melittin prevents liver cancer cell metastasis through inhibition of the Rac1-dependent pathway, *Hepatology* (Baltimore, Md.) 47 (2008) 1964-1973. 10.1002/hep.22240.
- [17] X. Cao, L. Zhang, Y. Shi, Y. Sun, S. Dai, C. Guo, F. Zhu, Q. Wang, J. Wang, X. Wang, Y.H. Chen, L. Zhang, Human tumor necrosis factor (TNF)-alpha-induced protein 8-like 2 suppresses hepatocellular carcinoma metastasis through inhibiting Rac1, *Mol Cancer* 12 (2013) 149. 10.1186/1476-4598-12-149.

- [18] C.F. Mo, J. Li, S.X. Yang, H.J. Guo, Y. Liu, X.Y. Luo, Y.T. Wang, M.H. Li, J.Y. Li, Q. Zou, IQGAP1 promotes anoikis resistance and metastasis through Rac1-dependent ROS accumulation and activation of Src/FAK signalling in hepatocellular carcinoma, *Br J Cancer* 123 (2020) 1154-1163. 10.1038/s41416-020-0970-z.
- [19] P. Yan, H. Gong, X. Zhai, Y. Feng, J. Wu, S. He, J. Guo, X. Wang, R. Guo, J. Xie, R.K. Li, Decreasing CNPY2 Expression Diminishes Colorectal Tumor Growth and Development through Activation of p53 Pathway, *Am J Pathol* 186 (2016) 1015-1024. 10.1016/j.ajpath.2015.11.012.
- [20] H. Taniguchi, S. Ito, T. Ueda, Y. Morioka, N. Kayukawa, A. Ueno, H. Nakagawa, A. Fujihara, S. Ushijima, M. Kanazawa, F. Hongo, O. Ukimura, CNPY2 promoted the proliferation of renal cell carcinoma cells and increased the expression of TP53, *Biochem Biophys Res Commun* 485 (2017) 267-271. 10.1016/j.bbrc.2017.02.095.
- [21] D. Wang, Z.M. Wang, S. Zhang, H.J. Wu, Y.M. Tao, Canopy Homolog 2 Expression Predicts Poor Prognosis in Hepatocellular Carcinoma with Tumor Hemorrhage, *Cell Physiol Biochem* 50 (2018) 2017-2028. 10.1159/000495048.

Figure Legends

Figure 1 Forward genetic screen using the *SB* insertional mutagenesis system for modeling HCC-induced metastasis. **(A)** Schematic diagram illustrating the different transgenic mice used as either control (no active *SB* system) or experimental active *SB* mutagenesis groups. Newborn mice with various control or experimental genotypes were aged until moribund before sacrificed for downstream analyses. **(B)** Representative images of mouse livers at different ages (150- to 203-days and 305- to 316-days) demonstrating the progression of liver tumorigenesis. Arrowhead, hyperplastic nodule. Bar charts showing percentage of mice with liver tumors (**top**) and liver weight to body weight ratio percentage (**bottom**) in different groups. Dashed line indicates average normal adult mouse liver percentage. *n*, number of animals. **(C)** Representative live images of liver tumors and lung metastases taken from same experimental mouse (**left panels**). Scale bar, 0.5 cm. Representative hematoxylin-eosin images of liver tumors and lung metastases taken from same experimental mouse (**right panels**). Scale bar, 100 μ m. N, adjacent normal parenchymal lung; T, liver tumor in alveoli.

Figure 2 Conditional *SB* insertional mutagenesis induced liver malignancy and lung metastasis in experimental mice. **(A)** Representative RT-PCR analyses of liver tumors and lung metastases taken from the same animal exhibiting active *SB* insertional mutagenesis system as shown by the detection of SB11 transposase (*SB*) and the expression of hepatocyte-specific markers such as *Fah* and *Alb*. *Actb*, housekeeping gene. **(B)** Representative immunohistochemical staining of liver tumors and lung metastases taken from the same mouse for *SB* transposase and liver-specific FAH. N, adjacent normal parenchymal lung; T, liver tumor in alveoli. Scale bars, 100 μ m.

Figure 3 Transposon-endogenous gene fusion transcripts identified in primary liver tumors and secondary lung metastases by RNA-seq. (A) Diagrammatic illustration of *Egfr* exon 24 and mutagenic transposon splice acceptor/polyadenylation tail (SA/pA) fusion transcript identified by RNA-seq. The T2/Onc mutagenic transposon was inserted into intron 24 in a reverse orientation, relative to the endogenous *Egfr* transcriptional direction. SD, splice donor; IR/DR, inverted repeats/direct repeats; MSCV 5' LTR, murine stem cell virus 5' long terminal repeat. (B) RNA-seq results showing the transcriptional expression profile of *Egfr* in both liver tumors and lung metastases using Integrative Genomics Viewer (IGV) software. Red arrow, location of *Egfr* exon 24. (C) Diagrammatic illustration of *Actn2* exon 15 and oncogenic transposon splice donor (SD) fusion transcript identified by RNA-seq. The T2/Onc mutagenic transposon was inserted into intron 14 in a forward orientation, relative to the endogenous *Actn2* transcriptional direction. (D) RNA-seq results showing the transcriptional expression profile of *Actn2* exclusively in lung metastases using IGV software. Red arrow, location of *Actn2* exon 15. (E) RT-PCR genotyping of *Egfr* and *Actn2* in non-sequenced primary liver tumors and secondary lung metastases. RT-PCR genotyping demonstrating the recurrent detection of transposon-*Egfr* fusion transcripts in remaining non-sequenced primary liver tumors and secondary lung metastases. RT-PCR genotyping demonstrating transposon-*Actn2* fusion transcripts and transcriptional differences before and after the fusion site at exon 15 in secondary lung metastases. No transposon-*Actn2* fusion or endogenous *Actn2* transcripts were detected in primary liver tumors or wild-type liver. DDW, double-distilled water.

Figure 4 Effect of *ACTN2* variants on cellular invasion and migration in HCC liver cancer cell line. (A) Representative images of truncated *ACTN2* (TAC), full length *ACTN2* (AC) and control (OFP) overexpressing vectors in transfected MHCC97L cells. Top panels, fluorescent microscopy for either GFP or OFP. Bottom panels, brightfield microscopy. Scale

bars, 100 μm . **(B)** Representative images for the effect of *ACTN2* variants and control overexpressing vectors on migration (**top panels**) and invasion (**bottom panels**) assays in transfected MHCC97L cells. Quantitative measurements of migration (**top graph**) and invasion abilities (**bottom graph**) by the intensity of stained penetrated cells using ImageJ software. *P*, unpaired *t*-test, *, $P < 0.05$; **, $P < 0.01$. Scale bars, 100 μm . **(C)** Summary diagram showing the hypothesized role of *CNPY2* and *ACTN2* in different stages of the metastatic process.

Figure A

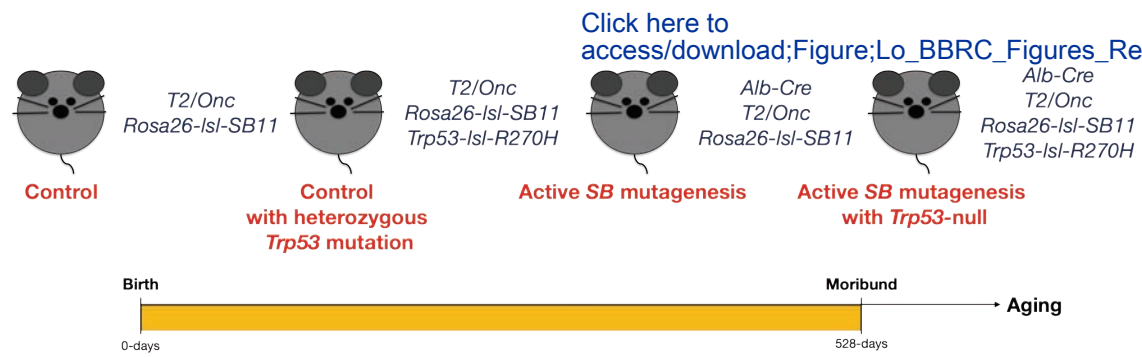
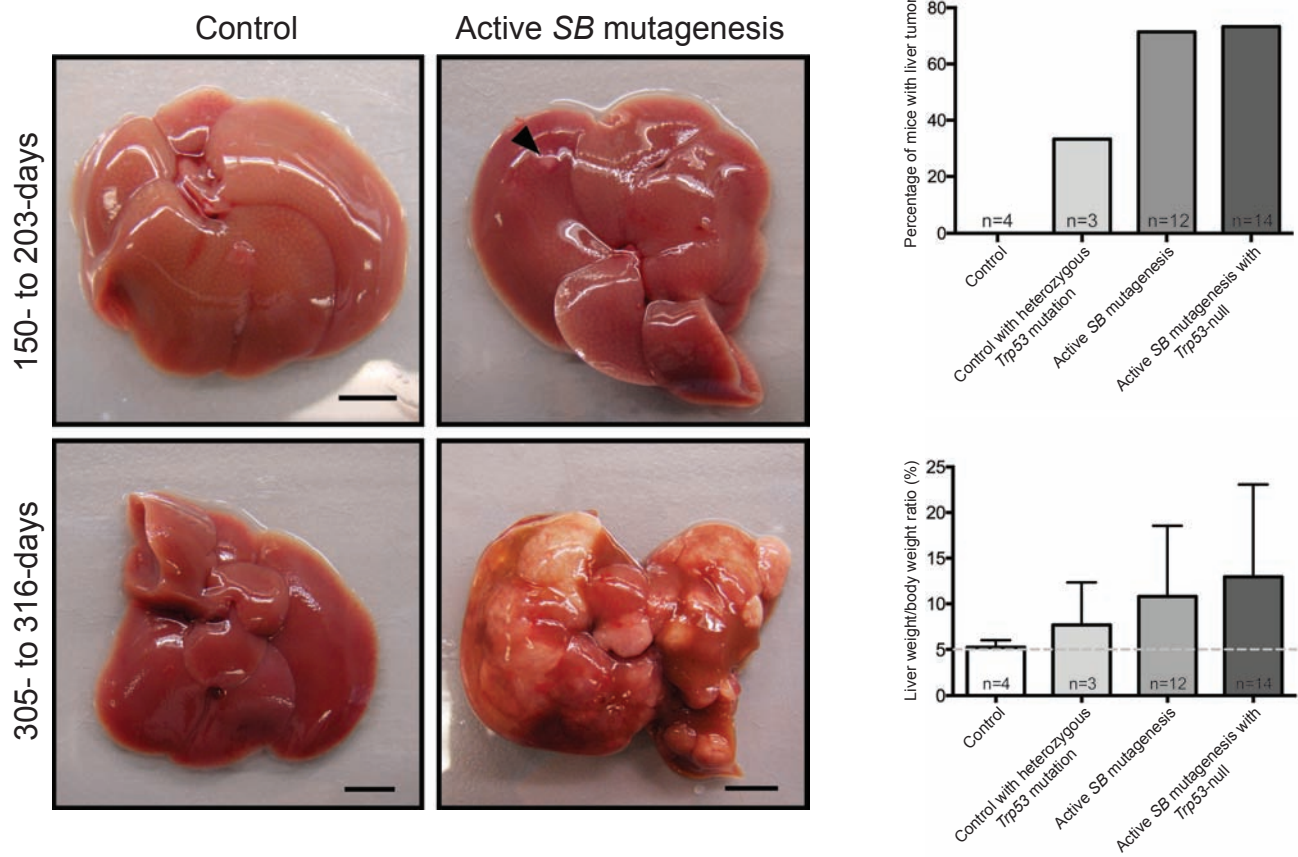
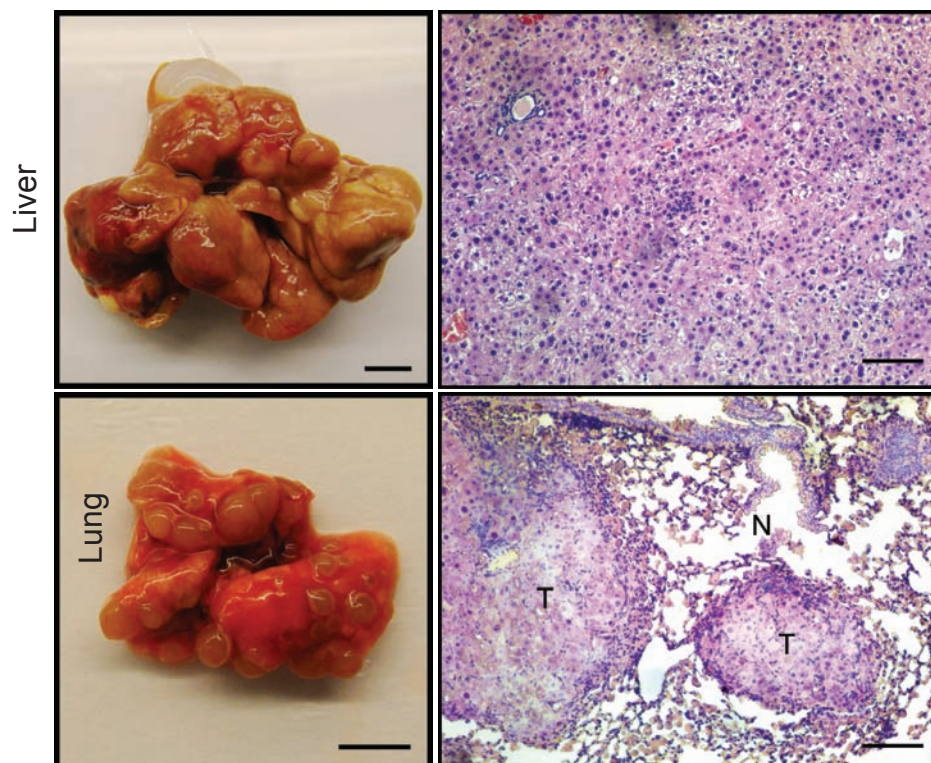


Figure 1

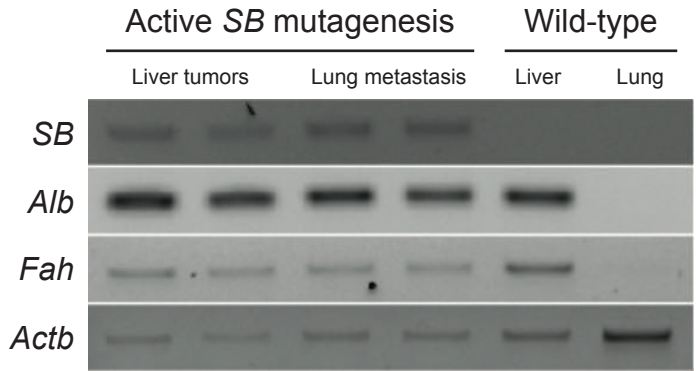
B



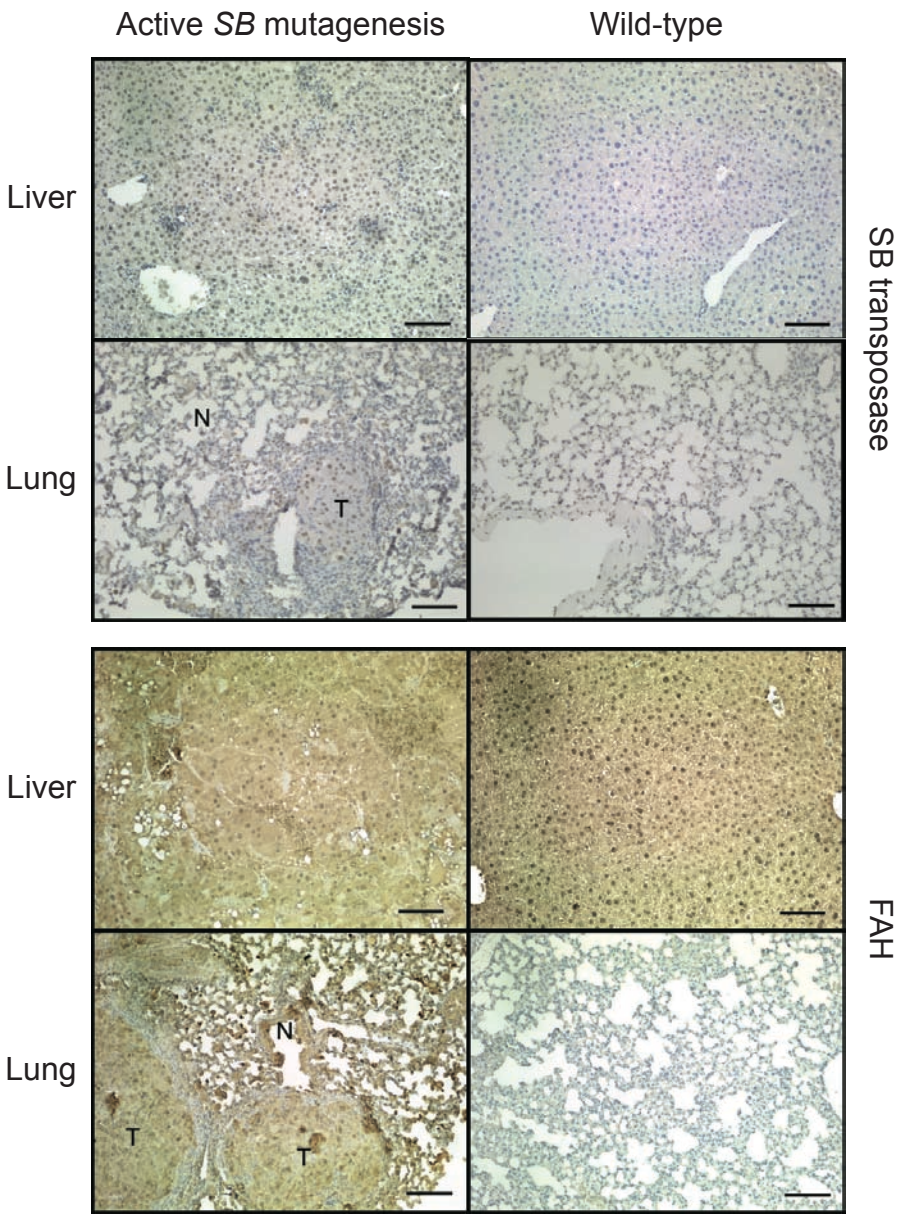
C



A



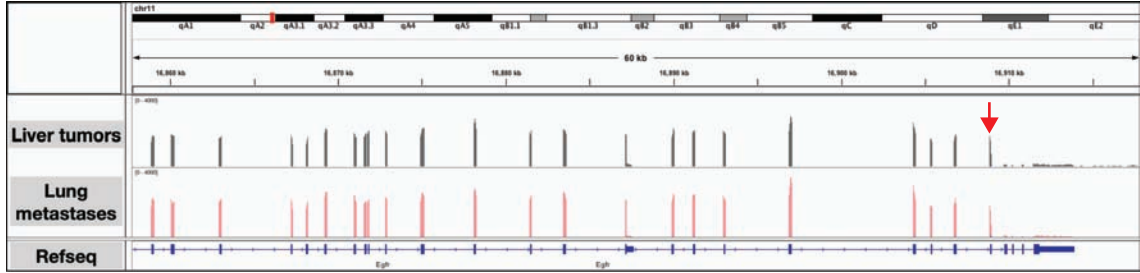
B



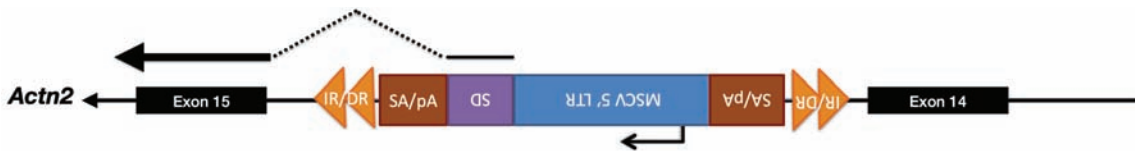
A



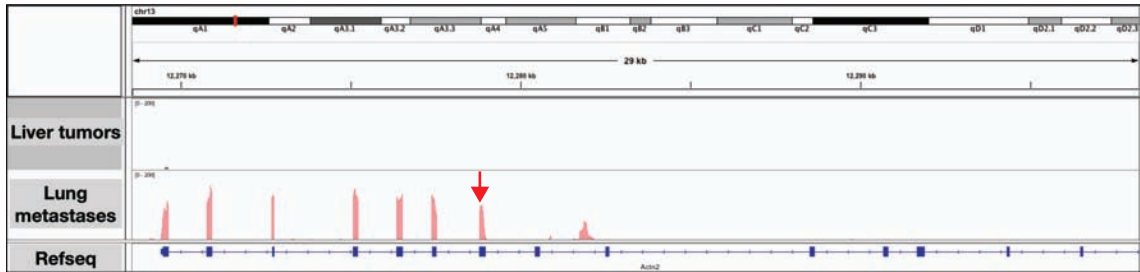
B



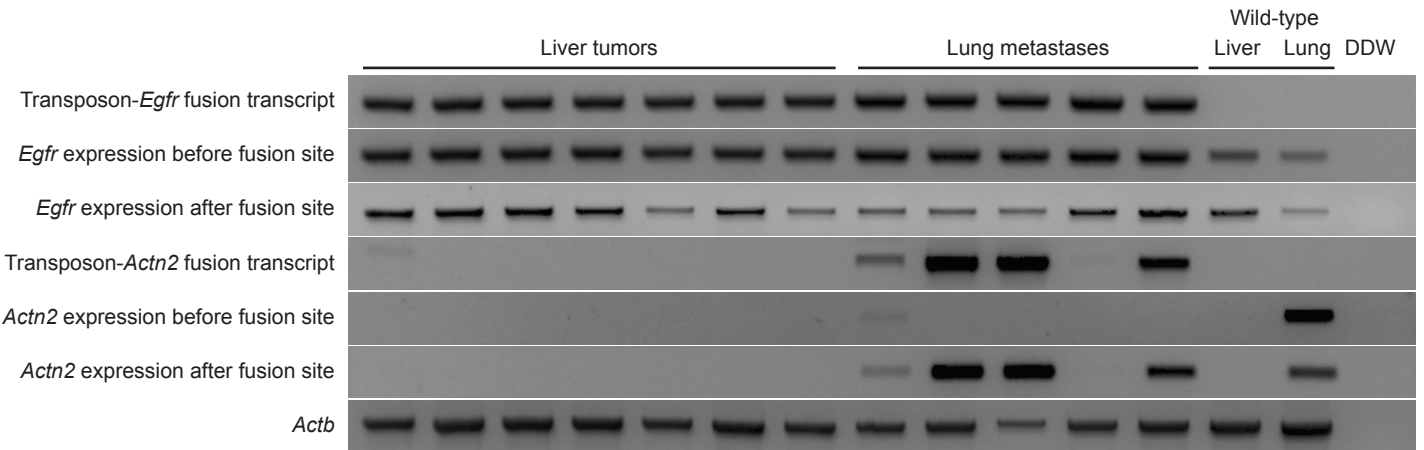
C



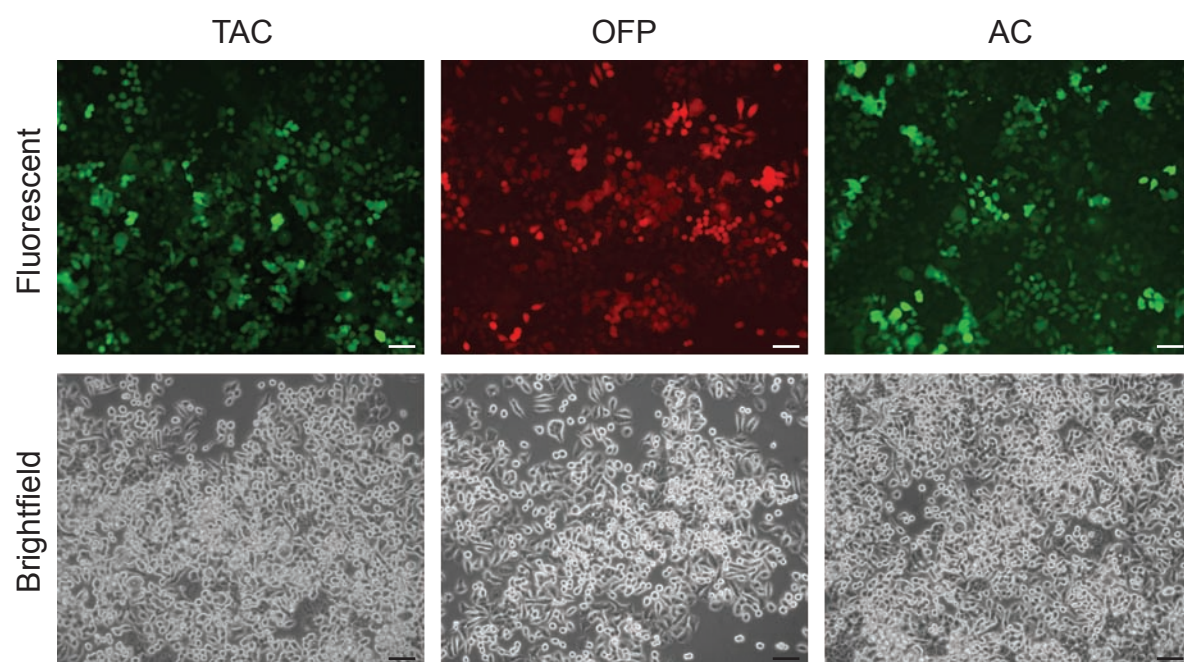
D



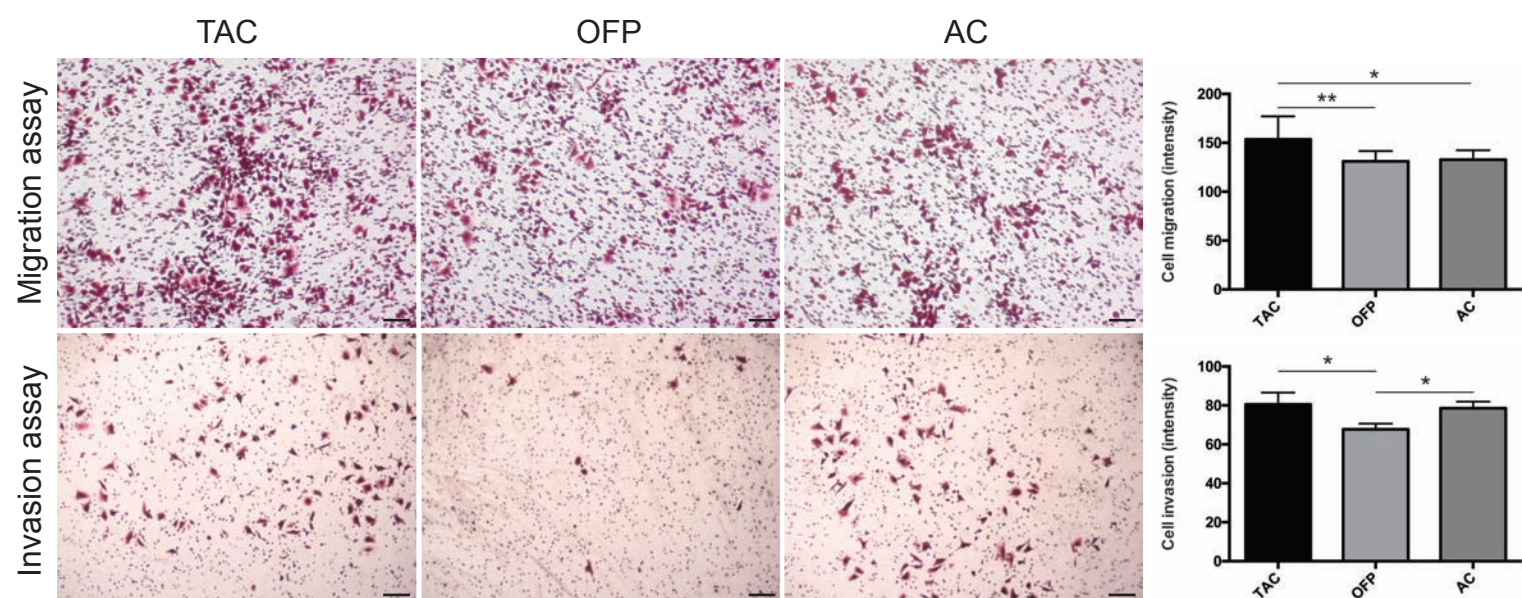
E



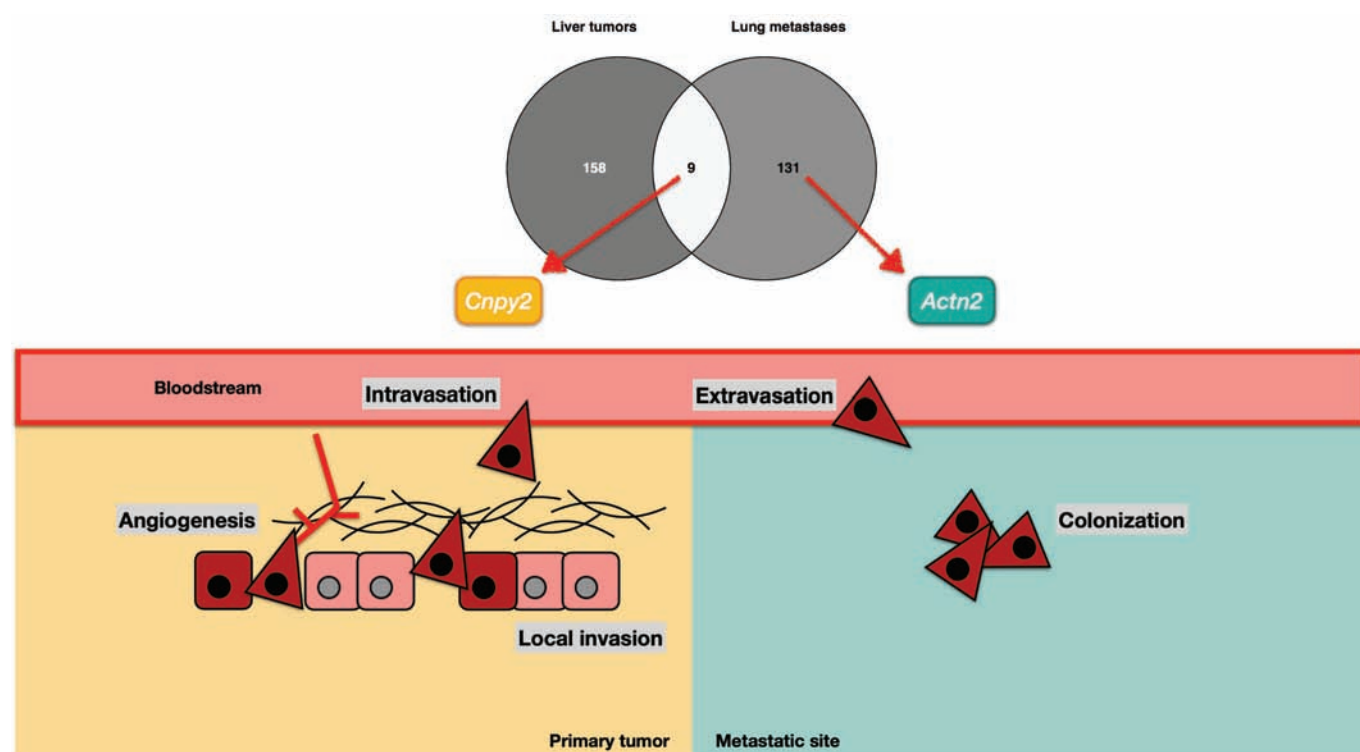
A



B



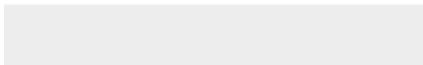
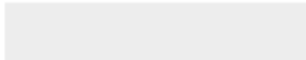
C





[Click here to access/download](#)

Supplementary Material (online publication only)
Lo_BBRC_Supplementary_Figures.pdf





[Click here to access/download](#)

Supplementary Material (online publication only)
Lo_BBRC_Supplementary_Tables.xlsx

